Plasmon-Enhanced Resonance Energy Transfer from a Conjugated Polymer to Fluorescent Multilayer Core–Shell Nanoparticles: A Photophysical Study

ARTICLE *in* THE JOURNAL OF PHYSICAL CHEMISTRY C · JANUARY 2011

Impact Factor: 4.77 · DOI: 10.1021/jp109993a

3 AUTHORS, INCLUDING:

Danny Brouard
Héma-Québec
6 PUBLICATIONS **94** CITATIONS

SEE PROFILE

Denis Boudreau
Laval University
49 PUBLICATIONS **1,433** CITATIONS

SEE PROFILE

THE JOURNAL OF PHYSICAL CHEMISTRY C

ARTICLE

pubs.acs.org/JPCC

Plasmon-Enhanced Resonance Energy Transfer from a Conjugated Polymer to Fluorescent Multilayer Core−Shell Nanoparticles: A Photophysical Study

Mathieu L.-Viger,[†] Danny Brouard,[†] and Denis Boudreau*

Département de chimie and Centre d'optique, photonique et laser (COPL), Université Laval, Québec (QC), Canada, G1 V 0A6

Supporting Information

ABSTRACT: The influence of metallic silver nanoparticles on Förster resonance energy transfer (FRET) between a water-soluble cationic conjugated polymer and fluorescent multilayer Ag@SiO_2@SiO_2+FiTC core−shell nanoparticles was characterized using a combination of light scattering and luminescence techniques. Positioning the fluorescent polymer 7 nm away from the surface of a 45 nm silver nanoparticle with a silica spacing layer increases its quantum yield to 77%, as compared to 3% when measured as an isolated emitter. In the presence of the metallic core, the luminescence of the nanoparticle-bound acceptor fluorophore is increased at the expense of the polymer donor luminescence, and time-resolved fluorescence measurements indicate an enhancement of FRET efficiency from 4 to 50%, an increase in the Förster distance from 50 to 85 Å, and a resonant transfer rate between donors and acceptors more than 2 orders of magnitude higher than that measured in the absence of the metal core. The strong influence of plasmonic coupling in these multilayer nanocomposites offers great potential for signal amplification schemes in polymer-based and FRET-based biosensors.

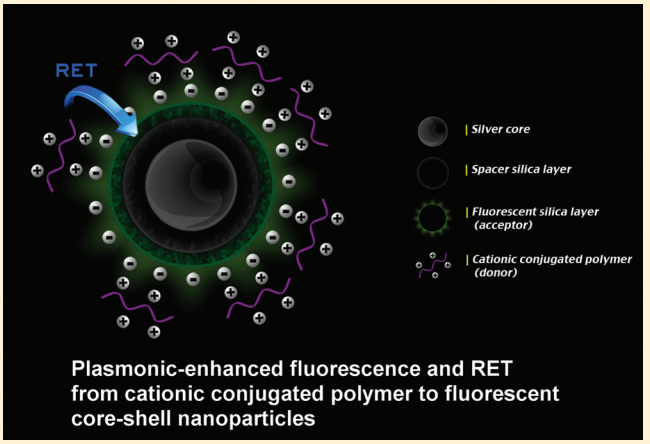

INTRODUCTION

Conjugated polymers (CPs) are attracting considerable attention on account of the rapidly growing number of applications in which they are being used,[1] including the development of transistors,[2−4] flexible photovoltaic devices,[5,6] light-emitting diodes,[7,8] and optical biosensors.[9] Among these fields of application, the latter is arguably one of the most promising. For instance, water-soluble polythiophene derivatives are known for their capacity to recognize and report different biological moieties in aqueous media such as oligonucleotides and proteins.[10,11] The transduction mechanism responsible for such molecular recognition is based on "affinity chromism"; for example, in the case of DNA detection, certain cationic polymers can form electrostatic complexes with anionic oligonucleotides, inducing conformational changes of the conjugated backbone that affect the polymer's spectral attributes (e.g., batho-/ipsochromic wavelength shifts, intrachain quenching of luminescence, etc.). Given the intrinsically high sensitivity of fluorescence-based detection methods, such chromic effects have been instrumental in the development of very sensitive polymer-based fluorometric DNA detection schemes.[12−15]

Although progress in modern synthetic chemistry has led to synthesis of various well-defined CPs with optimized photophysical properties, many CPs offer insufficient photoluminescence and photostability. For instance, the presence of conjugation-breaking defects along the polymer chain can lower the fluorescence quantum efficiency by favoring nonradiative pathways.[16] Therefore, the continued development of sensitive conjugated polymer-based biosensing schemes relies on the investigation of novel strategies to enhance the optical response of CPs.

In this regard, metal nanostructures are known to exhibit remarkable optical properties, owing to the surface plasmon modes sustained by their conduction electrons, such that the interactions between these plasmons and nearby fluorescent molecules are known to influence the molecules' electronic transition rates.[17,18] Localized surface plasmon resonance (LSPR) can lead to significant increases in fluorescence from a nearby fluorophore when quenching by the metal via charge- and energy-transfer processes at close range is prevented. Therefore, precise control of the distance between fluorophores and the metallic surface is important to achieve significant enhancement.[19,20]

The integration of noble metal nanoparticles with molecular fluorophores into composite nanostructures where fluorescent

Received: October 18, 2010
Revised: December 7, 2010
Published: January 11, 2011

molecules are precisely positioned relative to the nanoparticle surface provides many of the main features required of an ideal biosensor, that is, high optical detection sensitivity, excellent chemical and photophysical stability, low toxicity, high solubility in water, and easy conjugation to target biomolecules and/or fluorophores.[21−25] Whereas the metal core imparts strong LSPR to the composite nanoparticle, the growth of a controlled-thickness dielectric silica layer around the core provides a robust method to control the dye−metal separation and optimize fluorescence enhancement. In addition, the surface of this silica layer can be functionalized to covalently link fluorophores or form electrostatic complexes with charged molecules such as CPs. This represents a valuable strategy for enhancing the luminescence efficiency of surrounding molecules by improving their absorption and emission rates, while the plasmon-induced reduction of their lifetime in the excited state increases their photostability and detectability.[26−28]

Metal nanoparticles are also capable of influencing Förster resonance energy transfer (FRET) between two molecules. This nonradiative mechanism occurs between the oscillating dipoles of closely spaced molecules (<10 nm) when the donor's emission overlaps the acceptor's absorption band. FRET is often used as a spectroscopic ruler to estimate nanometer-scale distances within or between macromolecules.[29,30] Recent theoretical and experimental works have shown that positioning donor−acceptor pairs close to metal nanoparticles results in an enhancement of transfer rate, along with an increase in the efficiency and range of FRET.[31−34] CPs are known to be excellent energy donors for FRET and have been studied in FRET-based biodetection techniques.[35,36] Due to their delocalized electronic structure, CPs can transfer the excitation energy along their conjugated backbone to a high quantum yield acceptor, resulting in the amplification of the overall fluorescence signal. For instance, Ho et al.[37] used a fluorescence signal amplification mechanism based on the formation of aggregates between a cationic conjugated polymer (CCP) and fluorophore-labeled DNA probes to achieve ultrasensitive DNA detection, and further studies have shown that this high sensitivity was due to the capacity of the CCP to transfer energy to a large number of acceptor dye molecules within the aggregates. Bazan et al.[12] have devised similar FRET-amplified CP-based detection schemes for highly sensitive and specific detection of DNA. Given the advantageous features of plasmonic-enhanced FRET, as noted above, it is reasonable to postulate that the combination of plasmon-enhanced FRET with CPs could yield significantly improved detection sensitivity in polymer-based biosensing schemes.

In the present work, we studied the characteristics of a water-soluble CCP adsorbed on silver-core−silica-shell nanoparticles. The fine control in core diameter and core/acceptor/donor distances, provided by a versatile multilayer core−shell concentric architecture, facilitated the investigation of the photophysical processes involved in plasmon-modified FRET between the CCP and the fluorescent nanoparticles. Steady-state and time-resolved fluorescence were used to investigate the enhancement in the efficiency of energy transfer in such composite nanostructures.

EXPERIMENTAL SECTION

Materials. The CCP (poly(1H-imidazolium, 1-methyl-3-[2-[(4-methyl-3-thienyl)oxy]ethyl]-, chloride)), synthesized according to the procedure published previously,[38] was graciously provided by the group of Prof. Mario Leclerc and used as received. It has an average molecular weight of 11 000 g/mol with a polydispersity index of 2.0 and possesses one positive charge per monomer unit of 262.83 g/mol. Silver nitrate ($AgNO_3$, Aldrich), sodium citrate tribasic dihydrate (Na-Cit, Aldrich), tetraethoxysilane (TEOS, Aldrich), ammonia (NH_4OH 30%, Aldrich), fluorescein *i*-thiocyanate (FiTC, Aldrich), 3-(aminopropyl)triethoxysilane (APS, Aldrich), succinic anhydride (SA, Aldrich), and sodium chloride (NaCl, Aldrich) were used as received; 18 MΩ deionized water, anhydrous ethanol (EtOH), and anhydrous *N*,*N*-dimethylformamide (DMF, Aldrich) were used as dispersion media.

Synthesis of Ag@SiO_2 and FiTC-Doped Ag@SiO_2@SiO_2+FiTC Core−Shell Nanoparticles and Preparation of Nanoshell Control Samples. The synthesis of Ag@SiO_2 core−shell nanoparticles (NPs) and Ag@SiO_2@SiO_2+FiTC fluorescent multilayer core−shell NPs was performed following a protocol described elsewhere.[20] Typically, silver NPs with an average size of ∼45 nm were prepared by reduction of $AgNO_3$ with Na-Cit, and a 7 nm thick silica spacer shell was grown on these silver cores using an adaptation of the Stöber method (Figures 1a and 3). This particular spacer shell thickness was chosen according to a previous study[20] in which the influence of the distance between the metal core and surrounding fluorophores was investigated for various spacer shell thicknesses, and the highest fluorescence enhancement was obtained for a 7 nm thick spacer. These Ag@SiO_2 NPs were used either for the preparation of CCP/Ag@SiO_2 nanocomposites (see the following section) or for deposition of the FiTC-doped silica shells. The second silica shell containing covalently grafted FiTC molecules was deposited on the Ag@SiO_2 nanocomposites using a FiTC-conjugated silane coupling agent (Figure 1b) referred herein as APS-FiTC. The fluorescent nanoparticles were used either for spectroscopic measurements or for the preparation of CCP/Ag@SiO_2@SiO_2+FiTC nanocomposites (see section below). One should note that the amount of APS-FiTC used in this synthesis was adjusted to yield the highest fluorescence signal from the fluorescent core−shell nanoparticles with regards to concentration quenching and corresponds to a FiTC concentration in the silica shells of ∼10 mM and a labeling ratio of ∼10%. The hollow silica nanoshell control samples (Figure 1c) were prepared from core−shell nanoparticles by dissolution of the silver core with chloride ions,[20] and the silica nanoparticles (diameter = ∼50 nm) were prepared according to ref 39.

Preparation of CCP/Ag@SiO_2 Complexes. Deposition of the CCP onto core−shell nanoparticles (Figure 1d) follows a very simple procedure. First, a stock polymer solution of 8.4×10^{-4} M (calculated on a monomeric basis) was obtained by dissolving 2.2 mg of polymer in 10 mL of 18 MΩ deionized water; 20 μL of this polymer solution was added to 1 mL of core−shell nanoparticles. After an incubation period of 30 min at room temperature, the CCP/Ag@SiO_2 NPs were collected by centrifugation, washed three times with water, and dispersed in 1 mL of water. One must note that the same method was also used to obtain the CCP/SiO_2 NPs. Because the absorption and fluorescence spectra of CCP/Ag@SiO_2 electrostatic complexes are strongly distorted by the presence of the silver core, the binding capacity of the CCP onto the NPs was determined by measuring the amount of polymer adsorbed onto plain silica NP surrogates. The bound CCP was found to be $(1.20 \pm 0.06) \times 10^{-21}$ mol of polymer chains/NP or $(7.2 \pm 0.4) \times 10^2$ polymer chains/NP. Those numbers can be extrapolated to core−shell NPs because they share the same surface area, chemical structure, and surface properties.

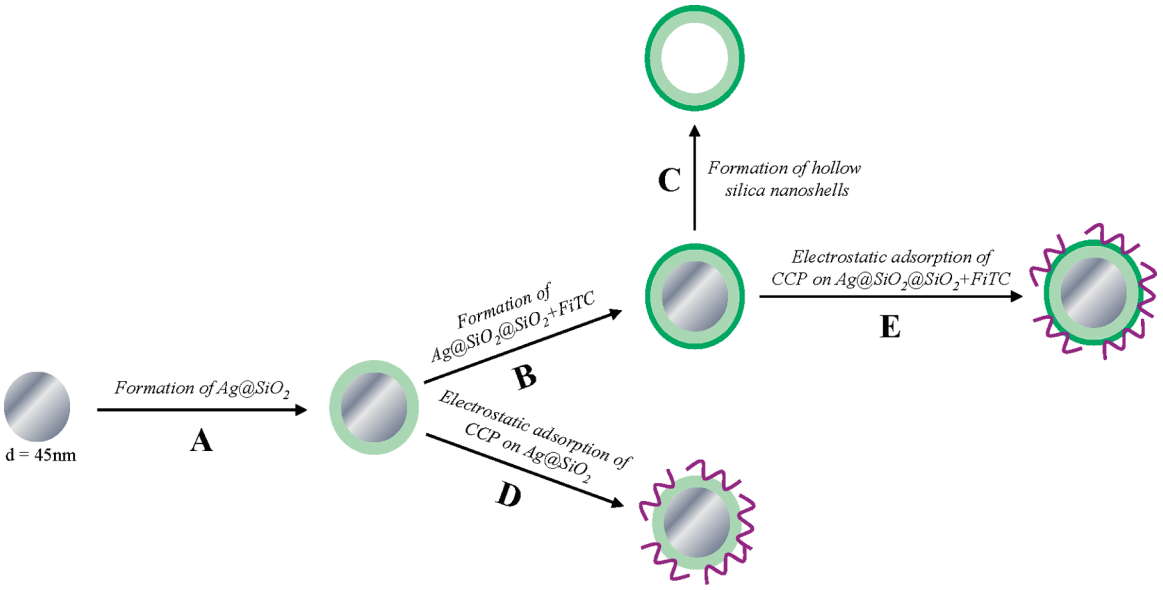

Figure 1. Schematic representation of the various nanoarchitectures used in this study.

Preparation of CCP/Ag@SiO_2@SiO_2+FiTC Electrostatic Complexes. Because a slight excess of APS was used in the synthesis of the FiTC-conjugated silane coupling agent, primary amine groups are expected to be present on the surface of fluorescent core−shell nanoparticles. At the nominal pH of deionized water, the primary amines ($pK_a \approx 10$) are assumed to be protonated and carry a positive charge. Consequently, the CCP cannot be deposited directly on the surface of fluorescent core−shell NPs. Therefore, succinic anhydride was used to convert the amine groups into carboxylate groups ($pK_a \approx 5$). Typically, 1 mL of fluorescent core−shell nanoparticle solution was centrifuged and redispersed in 1 mL of DMF followed by the addition of 100 μL of a 50 mM succinic anhydride solution in DMF. The mixture was stirred for 4 h at room temperature. The carboxylate-functionalized NPs were collected by centrifugation, washed three times with water, and redispersed in 1 mL of borate buffer at pH 9. Finally, 20 μL of polymer solution was added to 1 mL of core−shell nanoparticles and incubated for 30 min at room temperature. The CCP/Ag@SiO_2@SiO_2+FiTC nanocomposites (Figure 1e) were collected by centrifugation, washed three times with water, and redispersed in 1 mL of borate buffer at pH 9.

Spectrophysical Characterization. Transmission electron microscopy (TEM, Model JEM-1230, JEOL Instruments) was used to study the size, morphology, and structure of the core−shell nanoparticles. Nanoparticle samples were observed on Formvar films (Fluka) supported by nickel hexagonal 200 mesh grids (SPI supplies). Zeta potential measurements were done using a Malvern Zetasizer Model 3000 HSA. The fluorescence imaging experiments were performed using an optical microscope (BX-51, Olympus) in epifluorescence mode equipped with a Xenon lamp (LB-LS/30, Sutter Instrument Company) and a fluorescence mirror unit (U-MWBV2). The light emitted by the nanoparticles was collected by a 40× dry objective (UPlanFLN, N.A. = 0.75, Olympus), and images were acquired using a 1.4 megapixel CCD color digital camera (Infinity 2, Lumenera Corp). Aqueous nanoparticle aliquots were deposited on standard microscope slides cleaned by sonication in ethanol, dried under a nitrogen flow, and finally treated with a polymer-based cleaning solution (First Contact Polymer, Photonic Cleaning Technologies, Inc.). Recorded fluorescence images were processed using commercial image analysis software (IMT i-Solution). Steady-state fluorescence measurements were performed on a Fluorolog 3 spectrofluorometer (Model 322) from Horiba Jobin-Yvon featuring double monochromators on the excitation and emission channels and a Peltier-cooled R928P PMT detector. Fluorescence lifetime measurements were performed on a FluoTime 200 TCSPC time-resolved fluorescence platform from Picoquant GmbH (Berlin, Germany) equipped with a violet (405 nm) picosecond pulsed laser diode source (Becker & Hickl, BDL-405) and a Peltier-cooled MCP-PMT detector (Hamamatsu). The pulse repetition rate was 20 MHz, and the instrument response function (IRF) fwhm (full width at half maximum) was 72 ps. Fluorescence lifetimes were extracted from the decay curves using commercially available fluorescence lifetime analysis software (FluoFit Pro, PicoQuant GmbH). The UV−vis absorption spectra were measured on a Varian Cary 50 spectrophotometer.

RESULTS AND DISCUSSION

The hydrophilic nature and high charge density of the cationic polythiophene derivative used in this study are the result of the cationic side chains present on the polymer. In solution, the CCP adopts a random coil conformation and has a quantum yield of 3%.[38] It is characterized by a remarkably large Stokes shift between the excitation and emission maxima at 400 and 520 nm, respectively (Figure 2). This CCP presents an affinity chromism that has been studied extensively by the Leclerc group.[10]

The influence of plasmonic coupling on the fluorescence properties of the CCP was investigated using spherical Ag@SiO_2 core−shell NPs having an average core size of ∼45 nm and a spacer shell thickness of ∼7 nm (Figure 3).[20] Silver was preferred as the core material to other noble metals such as gold because of its 5 times higher extinction coefficient. In addition, it is well-known that a direct correlation exists between the extent of plasmon enhancement of fluorescence and the degree of spectral overlap between the plasmon absorption band of the NP and the excitation band of the fluorophore,[40] and the plasmon band of Ag NPs, centered at 400 nm, overlaps perfectly with the absorption band of the CCP (Figure 4).

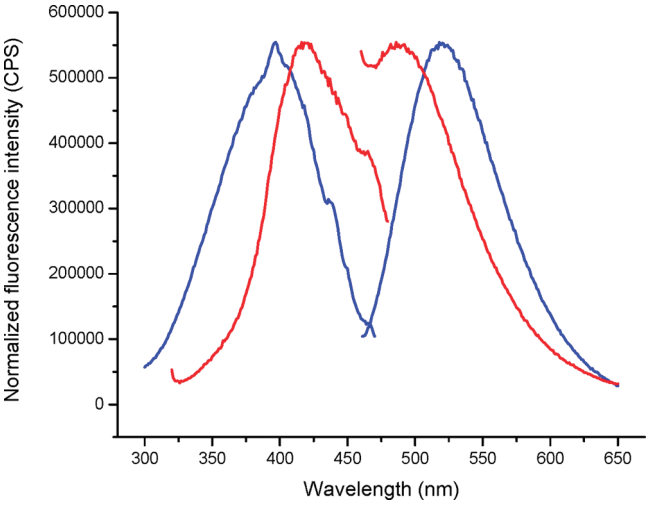

Figure 2. Excitation−emission spectra of the cationic conjugated polymer (CCP) in water (blue curves) and as CCP/Ag@SiO_2 electrostatic complexes (red curves).

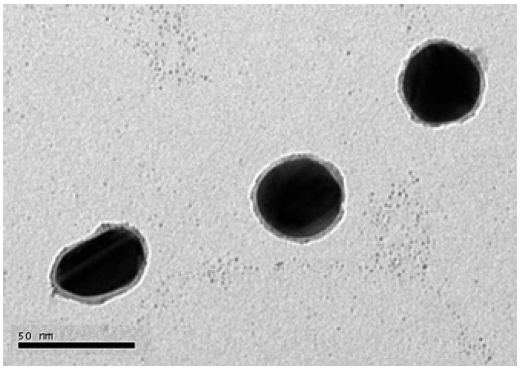

Figure 3. Transmission electron microphotographs of Ag@SiO_2 core−shell nanoparticles.

Silica surfaces in water acquire a negative charge due to the deprotonation of weakly acidic silanol groups, which was confirmed by zeta potential measurements for Ag@SiO_2 NPs (ζ = −8.5 mV). The pronounced positive charge of the CCP dispersed in pure water (ζ = +44.6 mV) favors the formation of CCP/Ag@SiO_2 complexes by electrostatic interaction, with a measured ζ potential of +10.3 mV. Fluorescent CCP/Ag@SiO_2 NPs and silica NP control samples (CCP/SiO_2) obtained by this simple procedure are compared in Figure 5.

Electrostatic complexation of the CCP onto core−shell NPs or silica NPs leads to a +20 nm bathochromic shift in the excitation spectrum of the CCP, as well as a −30 nm ipsochromic shift of the emission band maximum (Figure 2). The observed blue shift in emission is attributed to changes in the conjugated backbone structure. When the CCP/Ag@SiO_2 complexes are formed, the electrostatic bonds created between the polymer chain and the silica surface reduce the effective conjugation length in the polymer chain by twisting the conjugated backbone, which is manifested by the observed increase in band gap energy.[41] The red shift noted for the excitation band could be due to the lowering of the energy of the CCP's excited state caused by increased proximity between neighboring fluorophores.[42]

The fluorescence properties of the polythiophene CCP adsorbed on core−shell NPs and on silica NPs were investigated.

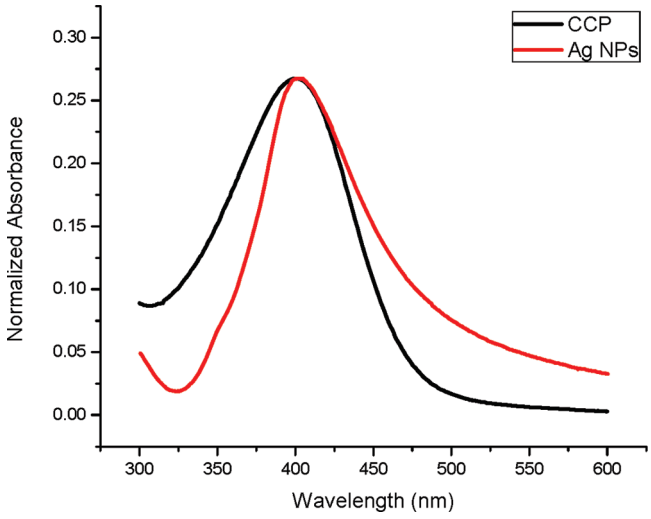

Figure 4. Spectral overlap between the excitation spectrum of the CCP (black curve) and the plasmon absorption band of silver nanoparticles (red curve).

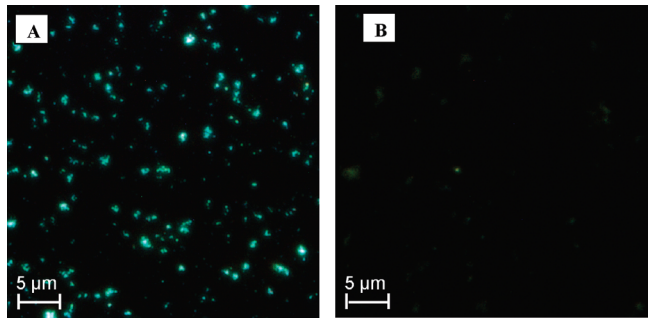

Figure 5. Optical epifluorescence microphotographs of (a) CCP/Ag@SiO_2 and (b) CCP/SiO_2 nanocomposites. The excitation wavelength is 420 ± 20 nm, and fluorescence above 500 nm is collected.

Fluorescence images recorded using epifluorescence microscopy show that the emission intensity is much higher when the CCP is in the presence of the metal core (Figure 5). To quantify the influence of plasmonic coupling on the fluorescence emission of the polymer, we monitored the fluorescence spectrum while adding increasing amounts of core−shell NPs to a constant concentration of CCP, which was fixed at a sufficiently low value to avoid loading the entire available NP surface and minimize the risk of interference caused by the inner filter effect at high NP concentration. Upon addition of Ag@SiO_2 NPs, we observed a gradual increase in fluorescence intensity, along with an abrupt shift of the emission band maximum toward shorter wavelengths (from 520 to 490 nm) as more CCP was bound to the NPs (Figure 6). The maximum fluorescence intensity measured at 490 nm for a concentration of 4.7×10^9 NPs/mL corresponds to a 27-fold increase in intensity as compared to the fluorescence intensity measured at 520 nm for the CCP free in solution. Upon further addition of NPs, the fluorescence emission spectra remained constant, indicating that the CCP was entirely complexed on the available surface, and eventually dropped due to inner filter effect. Interestingly, a similar behavior was also observed with the CCP/silica complexes, albeit registering only a 2-fold increase in fluorescence emission as compared to the CCP free in solution. Because both nanocomposites have the same surface composition,

dx.doi.org/10.1021/jp109993a |J. Phys. Chem. C 2011, 115, 2974–2981

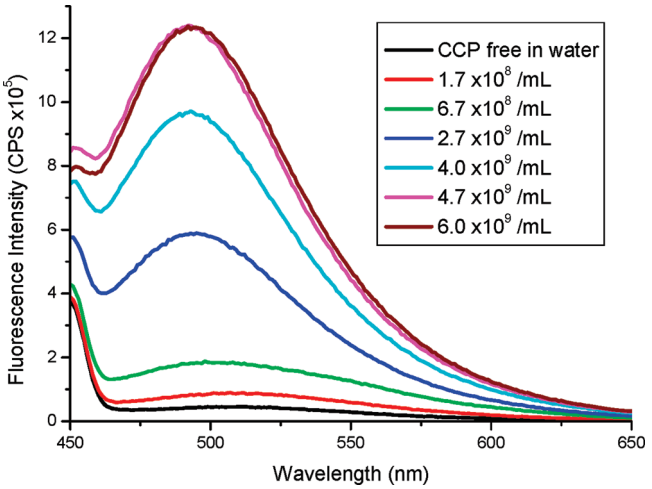

Figure 6. Influence of $Ag@SiO_2$ NP concentration on the fluorescence intensity of the cationic conjugated polymer. The polymer concentration was kept constant at 2.8×10^{-7} M on a monomeric basis unit for all measurements.

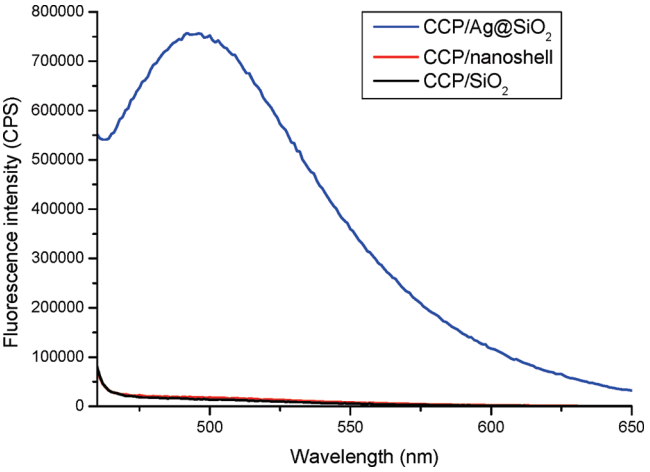

Figure 7. Steady-state fluorescence spectra for CCP adsorbed on $Ag@SiO_2$ NPs (blue curve), on hollow silica nanoshells (red curve), and on silica NPs (black curve). The excitation wavelength was 400 nm.

we can therefore postulate that the total fluorescence enhancement associated with the $CCP/Ag@SiO_2$ complexes arises from two distinct phenomena, the decrease in conjugation length responsible for a 2-fold increase and the plasmonic coupling accounting for a more substantial enhancement of fluorescence.

Comparison of the fluorescence spectra recorded for $CCP/Ag@SiO_2$ core−shell NPs with their respective nanoshell control samples, on the one hand, and with an equivalent concentration of CCP/SiO_2 NPs, on the other hand, yielded comparable ∼30-fold increases in fluorescence intensity in the presence of the metal core (Figure 7). This plasmon-enhanced fluorescence is the result of two different processes, that is, increases in the rate of excitation and in the rate of radiative decay, each having an influence on the apparent fluorescence quantum yield. An accurate description of the mechanism behind this enhancement requires the knowledge of the influence of metal-enhanced molecular absorptivity on the fluorescence data, that is, determination of the absorption cross section in the presence and in the absence of the metal core. In principle, this can be obtained by deconvoluting the absorbance due to the fluorophore from the overall extinction spectrum of the core−shell NPs. In the present case, however, efforts in this direction were thwarted by the strength of the silver particles' plasmon absorption band, which is orders of magnitude greater than the molecular absorption band of the CCP with which it overlaps. This obstacle was overcome using time-resolved fluorescence to measure the enhancement in the radiative decay rate induced by the metal particles because lifetime decay values are not affected by variations in absorptivity.

The lifetime of a fluorophore depends on its radiative decay rate; therefore, the increase in fluorescence noted previously for the $CCP/Ag@SiO_2$ complexes should also result in a shortening of the excited-state lifetime. This was confirmed by the measurement of a fluorescence lifetime of 28 ps measured for $CCP/Ag@SiO_2$ NPs, which corresponds to a ∼7-fold reduction in lifetime as compared to that for the CCP free in solution (Table 1 and Figure S1 in Supporting Information). Because photodegradation occurs while the fluorophore is in the excited state, a decrease in fluorescence lifetime should result in increased photostability of the fluorophore. In other words, CCP molecules located close to the metal colloids can undergo more

Table 1. Fluorescence Lifetime Data for CCP Free in Solution and as CCP/SiO_2, $CCP/Ag@SiO_2$, and $CCP/Ag@SiO_2@SiO_2$+FiTC Nanoparticles

	τ_1(ns)	A_1 (%)	τ_2(ns)	A_2 (%)	τ_{av} (ns)	χ^2
free in solution[a]	0.188	100			0.188	1.008
CCP/SiO_2[b]	0.119	100			0.119	1.003
$CCP/Ag@SiO_2$[b]	0.028	100			0.028	1.009
$CCP/Ag@SiO_2@SiO_2$+FiTC[b]	0.014	99.98	0.81	0.02	0.014	1.020

[a] λ_{ex} = 405 nm; λ_{em} = 530 nm. [b] λ_{ex} = 405 nm; λ_{em} = 490 nm.

excitation−relaxation cycles prior to photobleaching, resulting in a substantial increase in the number of detectable photons. When comparing the fluorescence lifetime of the CCP free in solution with that of the CCP bound to plain silica NPs, we measured a 1.6-fold decrease attributable to self-quenching between closely packed CCP molecules. Interestingly, the average intermolecular distance between CCP molecules on the silica particles, calculated from the concentration data, is ∼33 Å, which is comparable with the critical Förster distance calculated, using the formalism described below, for homotransfer between CCP molecules, that is, 37 Å.

The quantum yield (Φ) and lifetime (τ) of a fluorophore can be expressed as:

$$\Phi = \frac{\Gamma}{\Gamma + k_{nr}} \quad (1)$$

$$\tau = \frac{1}{\Gamma + k_{nr}} \quad (2)$$

where Γ and k_{nr} are the radiative and nonradiative decay rates, respectively.[21] When plasmonic coupling between a fluorophore molecule and a metallic nanoparticle causes an increase in the molecular radiative decay rate by a factor of γ, the metal-enhanced quantum yield (Φ_M) and lifetime (τ_M) values become

$$\Phi_M = \frac{\gamma\Gamma}{\gamma\Gamma + k_{nr}} \quad (3)$$

$$\tau_M = \frac{1}{\gamma\Gamma + k_{nr}} \quad (4)$$

dx.doi.org/10.1021/jp109993a |J. Phys. Chem. C 2011, 115, 2974–2981

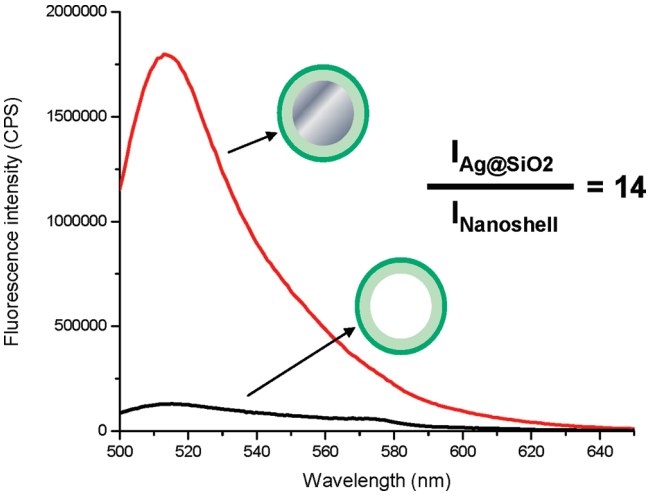

Figure 8. Fluorescence emission spectra of FiTC in $Ag@SiO_2@SiO_2$+FiTC nanocomposites (red curve) and in corresponding nanoshells (black curve). The excitation wavelength is 480 nm.

where $\gamma\Gamma$ represents the effective radiative decay rate.[21] The radiative rate ($\Gamma_M = \gamma\Gamma$) and quantum yield (Φ_M) of CCP/$Ag@SiO_2$ complexes can then be calculated from eqs 1−4 and the measure of the change in fluorescence lifetime caused by plasmonic coupling, using the assumption that the nonradiative decay rate k_{nr} is unaffected by the presence of the nanoparticle (given that the plasmon-driven component of the total nonradiative decay rate of a fluorophore near a metal surface scales as the inverse cubic power of the molecule−surface separation[43] and is known to be negligible for distances over 4 nm[44] versus the silica spacer of 7 nm used in the present work). A value of 77% was thus calculated for the metal-enhanced quantum yield Φ_M of the cationic polythiophene in CCP/$Ag@SiO_2$, as compared to 3% for the polymer free in water.

To establish a FRET system with these fluorescent CCP/$Ag@SiO_2$ core−shell NPs, an acceptor-labeled silica shell was deposited onto the silica-coated silver NPs prior to complexation with the fluorescent polymer. Fluorescein isothiocyanate (FiTC) was chosen as the energy acceptor because of its excellent spectral overlap with the emission band of the CCP. Using a fluorescent dye silica precursor, FiTC was covalently incorporated into a thin dye-doped silica shell at a concentration of approximately 10 mM (0.01 mol of fluorescein per kg of SiO_2). The luminescence of these FiTC molecules was also strongly affected by plasmonic coupling with the metal core, and a 14-fold increase in steady-state fluorescence intensity as well as a reduction in excited-state lifetime from 1.72 to 0.025 ns were measured for FiTC in $Ag@SiO_2@SiO_2$+FiTC NPs as compared with corresponding hollow silica nanoshells (Figure 8 and Table 2, also Figure S2 in Supporting Information). Interestingly, the lifetime of FiTC in the hollow silica nanoshells was shorter than that for FiTC free in solution (~4 ns). The quantum efficiency of most organic dyes is strongly affected by self-quenching when their concentration exceeds $\sim 10^{-3}$ M (a consequence of the higher probability of energy transfer between close pairs of dye molecules and between excited monomers and nonfluorescent dimers), which results in a decrease in fluorescence intensity and a reduction in fluorescence lifetime.[42] However, self-quenching can be suppressed by plasmonic coupling with metallic surfaces,[23] a phenomenon thoroughly studied by the group of Roux[45] and

Table 2. Fluorescence Lifetime Data for FiTC in $Ag@SiO_2@SiO_2$+FiTC Nanoparticles, in Corresponding Silica Nanoshell Samples, and Free in Solution

	τ_1 (ns)	A_1 (%)	τ_2 (ns)	A_2 (%)	τ_{av} (ns)	χ^2
FiTC in solution[a]	3.74	100			**3.74**	1.128
FiTC in $Ag@SiO_2@SiO_2$+FiTC[a]	3.55	0.1	0.023	99.9	**0.025**	1.015
FiTC in silica nanoshells[a]	3.45	47	0.190	53	**1.72**	1.184

[a] λ_{ex} = 480 nm; λ_{em} = 520 nm.

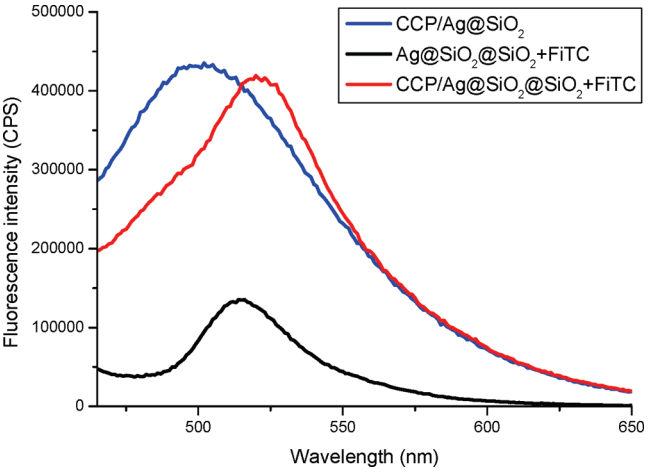

Figure 9. Comparison of fluorescence emission spectra recorded for CCP/$Ag@SiO_2$ (donor only), $Ag@SiO_2@SiO_2$+FiTC (acceptor only), and CCP/$Ag@SiO_2@SiO_2$+FiTC (donor−acceptor) nanocomposites. The excitation wavelength was 400 nm.

attributed to a strong decrease in nonradiative decay rates, that is, a reduction of energy transfer between dye molecules.

CCP donor molecules were adsorbed on acceptor fluorescent core−shell NPs to form CCP/$Ag@SiO_2@SiO_2$+FiTC nanocomposites. Figure 9 shows the fluorescence spectra recorded for the donor−acceptor nanocomposites and their corresponding donor-only and acceptor-only core−shell NPs. Upon excitation at 400 nm, the donor−acceptor nanocomposites displayed a reduction in donor emission intensity and a 5-fold increase in acceptor emission intensity. These results suggest the presence of efficient energy transfer from the surface-bound CCP to the encapsulated fluorescein. This was confirmed by the measurement of a decrease in donor lifetime, that is, from 28 to 14 ps (Table 1), and a distinctive red shift (5 nm) in the acceptor emission maximum for the donor−acceptor nanocomposites.

The lifetime of the donor alone (τ_D) and in the presence of the acceptor (τ_{DA}) are related to the FRET efficiency (E) by the following equation[46]

$$E = 1 - \frac{\tau_{DA}}{\tau_D} \quad (5)$$

A metal-enhanced efficiency (E_M) of 50% was calculated using eq 5 and the knowledge of the lifetime of CCP alone (τ_D) in CCP/$Ag@SiO_2$ (i.e., 28 ps) and in presence of FiTC (τ_{DA}) in CCP/$Ag@SiO_2@SiO_2$+FiTC (14 ps).

The Förster distance (R_0) for a FRET or homoFRET system (i.e., the distance at which the FRET efficiency is 50%) can be

calculated using the following relationship[46]

$$R_0 = 0.211[\kappa^2 \eta^{-4} \Phi_D J(\lambda)]^{1/6} \quad (6)$$

where κ^2 is the orientation factor (usually taken as 2/3 in non-oriented systems), η is the refractive index of the solution, Φ_D is the quantum yield of the donor, and $J(\lambda)$ is the overlap integral between the donor emission and the acceptor molar absorptivity, which can be calculated using the following equation[46]

$$J(\lambda) = \int_0^\infty F_D(\lambda)\varepsilon_A(\lambda)\lambda^4 \, d\lambda \quad (7)$$

where λ is the wavelength in nm, $F_D(\lambda)$ represents the normalized fluorescence intensity at a given wavelength, and $\varepsilon_A(\lambda)$ is the molar absorptivity of the acceptor at a given wavelength. Using eqs 6 and 7, an R_0 of 50 Å was calculated for the unaffected CCP/FiTC system (plain silica particles), and a metal-enhanced Förster distance ($R_{0(M)}$) of 85 Å using the quantum yield (Φ_M) of 77% was calculated for the CCP in CCP/Ag@SiO_2 nanocomposites. The transfer efficiency E_M of 50% and the metal-enhanced $R_{0(M)}$ of 85 Å determined for CCP/Ag@SiO_2@SiO_2+FiTC nanocomposites can be used to calculate a donor−acceptor distance (R) of 85 Å using the following relationship[46]

$$E = \frac{{R_0}^6}{{R_0}^6 + R^6} \quad (8)$$

Interestingly, from R = 85 Å and R_0 = 50 Å for the unaffected CCP/FiTC system, a 4% transfer efficiency in the absence of plasmonic interaction was calculated. Finally, from the knowledge of the plasmon-modified values for τ_D, R_0, and R and using eq 9[46]

$$k_t = \frac{1}{\tau_D}\left[\frac{R_0}{R}\right]^6 \quad (9)$$

a plasmon-enhanced donor−acceptor transfer rate of 3.6×10^{10} s^{-1} was obtained, which is 173 higher than that for an unaffected D−A pair. These results allow us to postulate that plasmonic coupling in the core−shell nanocomposites should allow the CCP to excite a larger number of acceptors over a given period of time and over distances exceeding the natural range of FRET measurements.

CONCLUSION

In this study, we investigated the effect of silver nanoparticles on the photophysical properties of a conjugated cationic polythiophene complexed with core−shell nanoarchitectures. The use of a protective silica layer with an adjustable thickness allows the precise tuning of dye−metal distances and of the extent of the interactions between core and fluorophores and between donor and acceptor. When compared with coreless control samples, these fluorescent NPs display an enhanced fluorescence quantum yield and shortened excited-state lifetimes, resulting in their much higher brightness. Moreover, the influence of plasmonic coupling on FRET was studied using a D−A pair composed of the conjugated polymer and an organic dye, fluorescein *i*-thiocyanate. When in close proximity to silver particles, the FRET efficiency is enhanced by a factor of 13 while the Förster distance is increased from 50 to 85 Å. Furthermore, the rate of energy transfer is found to be 173 times higher. The longer intermolecular interaction range and greater detectability manifested by these nanocomposites could have important applications in cell imaging and biosensing.

ASSOCIATED CONTENT

Supporting Information. Fluorescence lifetime analysis data. This material is available free of charge via the Internet at http://pubs.acs.org.

AUTHOR INFORMATION

Corresponding Author

*Phone: (418) 656-3287. Fax: (418) 656-7916. E-mail: denis.boudreau@chm.ulaval.ca.

Author Contributions

†Co-first authors that contributed equally to the work.

ACKNOWLEDGMENT

This work was supported by the Natural Sciences and Engineering Research Council of Canada, the "Fonds Québécois de la Recherche sur la Nature et les Technologies du Québec", the Canadian Foundation for Innovation, Héma-Québec, and the Canadian Blood Services. Also, the authors would like to acknowledge the contributions of Marie-Pier Blais for the cover artwork, Dr. Kim Doré (CRULRG, Université Laval) for stimulating discussions, Prof. Mario Leclerc (Dept. Chemistry, Université Laval) for the gift of the polymer and a long-standing collaboration on polymer-based biosensing, David Béliveau-Viel for MatLab calculations, Luc Rainville and Yoan LeChasseur for their contribution to the characterization of polymer/nanoparticle fluorescence, and, finally, Félix-Antoine Lavoie and Olivier Ratelle for the silica nanoparticles.

REFERENCES

(1) Leclerc, M.; Najari, A.; Beaupre, S. *Can. J. Chem.* **2009**, *87*, 1201–1208.
(2) Garnier, F. *Philos. Trans. R. Soc. London, Ser. A* **1997**, *355*, 815–827.
(3) Stutzmann, N.; Friend Richard, H.; Sirringhaus, H. *Science* **2003**, *299*, 1881–1884.
(4) Boudreault, P.-L. T.; Wakim, S.; Tang, M. L.; Tao, Y.; Bao, Z.; Leclerc, M. *J. Mater. Chem.* **2009**, *19*, 2921–2928.
(5) Kim, M.-S.; Kim, J.-S.; Cho, J. C.; Shtein, M.; Guo, L. J.; Kim, J. *Appl. Phys. Lett.* **2007**, *90*, 123113/01–123113/03.
(6) Li, G.; Shrotriya, V.; Huang, J.; Yao, Y.; Moriarty, T.; Emery, K.; Yang, Y. *Nat. Mater.* **2005**, *4*, 864–868.
(7) Burroughes, J. H.; Bradley, D. D. C.; Brown, A. R.; Marks, R. N.; Mackay, K.; Friend, R. H.; Burns, P. L.; Holmes, A. B. *Nature* **1990**, *347*, 539–541.
(8) Huang, C. C.; Meng, H. F.; Ho, G. K.; Chen, C. H.; Hsu, C. S.; Huang, J. H.; Horng, S. F.; Chen, B. X.; Chen, L. C. *Appl. Phys. Lett.* **2004**, *84*, 1195–1197.
(9) Gerard, M.; Chaubey, A.; Malhotra, B. D. *Biosens. Bioelectron.* **2002**, *17*, 345–359.
(10) Ho, H.-A.; Najari, A.; Leclerc, M. *Acc. Chem. Res.* **2008**, *41*, 168–178.
(11) Sigurdson, C. J.; Nilsson, K. P. R.; Hornemann, S.; Manco, G.; Polymenidou, M.; Schwarz, P.; Leclerc, M.; Hammarstroem, P.; Wuethrich, K.; Aguzzi, A. *Nat. Methods* **2007**, *4*, 1023–1030.
(12) Gaylord, B. S.; Heeger, A. J.; Bazan, G. C. *Proc. Natl. Acad. Sci. U.S.A.* **2002**, *99*, 10954–10957.
(13) Liu, B.; Bazan, G. C. *Chem. Mater.* **2004**, *16*, 4467–4476.
(14) Dore, K.; Dubus, S.; Ho, H.-A.; Levesque, I.; Brunette, M.; Corbeil, G.; Boissinot, M.; Boivin, G.; Bergeron, M. G.; Boudreau, D.; Leclerc, M. *J. Am. Chem. Soc.* **2004**, *126*, 4240–4244.
(15) Dore, K.; Leclerc, M.; Boudreau, D. *Rev. Fluoresc.* **2009**, *4*, 179–197.

(16) Saini, S.; Bagchi, B. *Phys. Chem. Chem. Phys.* **2010**, *12*, 7427–7433.
(17) Barnes, W. L. *J. Mod. Opt.* **1998**, *45*, 661–699.
(18) Aslan, K.; Gryczynski, I.; Malicka, J.; Matveeva, E.; Lakowicz, J. R.; Geddes, C. D. *Curr. Opin. Biotechnol.* **2005**, *16*, 55–62.
(19) Wokaun, A.; Lutz, H. P.; King, A. P.; Wild, U. P.; Ernst, R. R. *J. Chem. Phys.* **1983**, *79*, 509–514.
(20) Lessard-Viger, M.; Rioux, M.; Rainville, L.; Boudreau, D. *Nano Lett.* **2009**, *9*, 3066–3071.
(21) Bardhan, R.; Grady, N. K.; Cole, J. R.; Joshi, A.; Halas, N. J. *ACS Nano* **2009**, *3*, 744–752.
(22) Cheng, D.; Xu, Q.-H. *Chem. Commun.* **2007**, 248–250.
(23) Viger, M. L.; Live, L. S.; Therrien, O. D.; Boudreau, D. *Plasmonics* **2008**, *3*, 33–40.
(24) Tovmachenko, O. G.; Graf, C.; van den Heuvel, D. J.; van Blaaderen, A.; Gerritsen, H. C. *Adv. Mater.* **2006**, *18*, 91–95.
(25) Aslan, K.; Wu, M.; Lakowicz, J. R.; Geddes, C. D. *J. Am. Chem. Soc.* **2007**, *129*, 1524–1525.
(26) Tang, F.; He, F.; Cheng, H.; Li, L. *Langmuir* **2010**, *26*, 11774–11778.
(27) Pan, S.; Rothberg, L. J.; Nolte, A. J.; Rubner, M. F.; Gorodetskaya, I.; Swager, T. M. *Proc. SPIE—Int. Soc. Opt. Eng.* **2005**, *5927*, 592705/01–592705/08.
(28) Park, H.-J.; Vak, D.; Noh, Y.-Y.; Lim, B.; Kim, D.-Y. *Appl. Phys. Lett.* **2007**, *90*, 161107/01–161107/03.
(29) Bates, M.; Blosser, T. R.; Zhuang, X. *Phys. Rev. Lett.* **2005**, *94*, 108101/01–108101/04.
(30) Schuler, B.; Eaton, W. A. *Curr. Opin. Struct. Biol.* **2008**, *18*, 16–26.
(31) Reil, F.; Hohenester, U.; Krenn, J. R.; Leitner, A. *Nano Lett.* **2008**, *8*, 4128–4133.
(32) Zhang, J.; Fu, Y.; Chowdhury, M. H.; Lakowicz, J. R. *J. Phys. Chem. C* **2007**, *111*, 11784–11792.
(33) Zhang, J.; Fu, Y.; Lakowicz, J. R. *J. Phys. Chem. C* **2007**, *111*, 50–56.
(34) Xie, H. Y.; Chung, H. Y.; Leung, P. T.; Tsai, D. P. *Phys. Rev. B: Condens. Matter Mater. Phys.* **2009**, *80*, 155448/01–155448/10.
(35) Xing, C.; Xu, Q.; Tang, H.; Liu, L.; Wang, S. *J. Am. Chem. Soc.* **2009**, *131*, 13117–13124.
(36) Duan, X.; Liu, L.; Feng, F.; Wang, S. *Acc. Chem. Res.* **2010**, *43*, 260–270.
(37) Ho, H. A.; Dore, K.; Boissinot, M.; Bergeron, M. G.; Tanguay, R. M.; Boudreau, D.; Leclerc, M. *J. Am. Chem. Soc.* **2005**, *127*, 12673–12676.
(38) Ho, H.-A.; Boissinot, M.; Bergeron, M. G.; Corbeil, G.; Dore, K.; Boudreau, D.; Leclerc, M. *Angew. Chem., Int. Ed.* **2002**, *41*, 1548–1551.
(39) Jin, Y.; Lohstreter, S.; Pierce, D. T.; Parisien, J.; Wu, M.; Hall, C., III; Zhao, J. X. *Chem. Mater.* **2008**, *20*, 4411–4419.
(40) Chen, Y.; Munechika, K.; Ginger, D. S. *Nano Lett.* **2007**, *7*, 690–696.
(41) Leclerc, M. *Sens. Update* **2001**, *8*, 21–38.
(42) Imhof, A.; Megens, M.; Engelberts, J. J.; De Lang, D. T. N.; Sprik, R.; Vos, W. L. *J. Phys. Chem. B* **1999**, *103*, 1408–1415.
(43) Waldeck, D. H.; Alivisatos, A. P.; Harris, C. B. *Surf. Sci.* **1985**, *158*, 103–125.
(44) Soller, T.; Ringler, M.; Wunderlich, M.; Klar, T. A.; Feldmann, J.; Josel, H. P.; Markert, Y.; Nichtl, A.; Kuerzinger, K. *Nano Lett.* **2007**, *7*, 1941–1946.
(45) Martini, M.; Perriat, P.; Montagna, M.; Pansu, R.; Julien, C.; Tillement, O.; Roux, S. *J. Phys. Chem. C* **2009**, *113*, 17669–17677.
(46) Lakowicz, J. R. *Principles of Fluorescence Spectroscopy*, 2nd ed.; Plenum Publishing Corporation: New York, 1999.